Discontinuous percolation transitions in epidemic processes, surface depinning in random media, and Hamiltonian random graphs

Golnoosh Bizhani, Maya Paczuski, and Peter Grassberger
Complexity Science Group, University of Calgary, Calgary T2N 1N4, Canada
(Received 6 April 2012; revised manuscript received 6 July 2012; published 25 July 2012)

Discontinuous percolation transitions and the associated tricritical points are manifest in a wide range of both equilibrium and nonequilibrium cooperative phenomena. To demonstrate this, we present and relate the continuous and first-order behaviors in two different classes of models: The first are generalized epidemic processes that describe in their spatially embedded version—either on or off a regular lattice—compact or fractal cluster growth in random media at zero temperature. A random graph version of these processes is mapped onto a model previously proposed for complex social contagion. We compute detailed phase diagrams and compare our numerical results at the tricritical point in $d = 3$ with field theory predictions of Janssen *et al*. [Phys. Rev. E **70**, 026114 (2004)]. The second class consists of exponential ("Hamiltonian," i.e., formally equilibrium) random graph models and includes the Strauss and the two-star model, where "chemical potentials" control the densities of links, triangles, or two-stars. When the chemical potentials in either graph model are $\mathcal{O}(\log N)$, the percolation transition can coincide with a first-order phase transition in the density of links, making the former also discontinuous. Hysteresis loops can then be of mixed order, with second-order behavior for decreasing link fugacity, and a jump (first order) when it increases.

DOI: 10.1103/PhysRevE.86.011128 PACS number(s): 64.60.ah, 68.43.Jk, 89.75.Da

I. INTRODUCTION

Percolation describes the sudden appearance of systemwide connectivity arising from microscopic processes. It is a classic example [1] of a continuous ("second-order") phase transition. Interest in systems where the percolation transition is discontinuous ("first order") was sparked recently by claims for this in *Achlioptas processes* [2]. Although these transitions were later shown to be continuous [3–6]—albeit with unusual finite-size scaling behavior [5]—the fact that percolation transitions could be discontinuous was claimed to be novel [3,4,7–24]. After this, discontinuous percolation transitions were observed in interdependent networks [25–27], in models inspired by [2] but not using the Achlioptas trick [15–18], and in a hierarchical lattice [28].

One purpose of this work is to point out that discontinuous percolation transitions are not surprising and, indeed, are common to a variety of (e.g., social or physical) cooperative phenomena. The existence of such transitions, together with an associated tricritical point, was proposed 25 years ago [29] in the context of directed percolation. This was verified in the seminal field theoretic work of Janssen *et al*. [30] who introduced the *generalized epidemic process* (GEP) [31]. In this scenario, the continuous transition is just ordinary percolation (OP), while the discontinuous one is the depinning transition of driven surfaces in random media at zero temperature [32,33].

Although the latter is continuous from the point of view of surface properties, it is discontinuous so far as the percolation order parameter is concerned [34]. Indeed, the density of "wetted" sites in the presence of a driven interface jumps discontinuously from zero to a finite value at depinning.

A closely related line of papers finding discontinuous percolation transitions started independently in a social science context [35–37] and addresses complex contagion or epidemics in random networks. It turns out that the model of [36] is basically the random graph version of the GEP, as we explain in detail below. Our unified formulation based on GEP, that includes both social contagion and interface depinning, simplifies the description of both and isolates relevant variables that can affect the actual outcome in terms of potentially measurable observables.

We present numerical simulation results for the GEP, including the time dependence of the number of growth sites in three dimensions. At the first-order (=depinning) transition line, activity decays as a stretched exponential in time while it behaves as a power law both at the OP transition and at the tricritical point which separates rough from fractal growth. We give (tri-)critical exponents and compare them to theoretical predictions [30].

The main property that leads to first-order transitions in the models we consider is cooperativity (or "synergy") in establishing links. This cooperativity can be implemented technically in different ways. We do this via stochastic dynamics as in [30,35–37] for the GEP, and also via Gibbs-Boltzmann *equilibrium* distributions in Hamiltonian (or "exponential") ensembles, which have been used extensively to model social networks.

Indeed, we also find discontinuous percolation transitions in two exponential random graph models : the Strauss [38,39] and the two-star model [40]. They are both formulated in terms of a partition function and are generalizations of the standard Erdös-Renyi (ER) random graph [41]. The Hamiltonians are bilinear with a control parameter (θ) conjugate to the number of links and another control parameter conjugate to either the number of triangles or the number of "two stars." When all control parameters are $\mathcal{O}(\log N)$ (where N is the number of nodes in the graph), the percolation transition can be either continuous or discontinuous, with hysteresis loops typical of first-order transitions. But for certain parameter regimes unusual hysteresis loops occur, where the percolation order parameter exhibits second-order (singular but continuous) behavior for decreasing θ, but jumps discontinuously for increasing θ. Similar "mixed-order" hysteresis loops have been found in heterogeneous k-core percolation [42].

It is well known that the observation of continuity of a phase transition depends not only on the choice of the order parameter, but also on the choice of the control parameter. Take, for example, the standard example of a liquid-gas transition. If the temperature of water is increased at constant pressure, then the density and the free energy jump discontinuously at the boiling temperature. If, however, the volume is kept fixed, no such jump is observed. Instead, as temperature is increased, a larger and larger fraction of the sample turns into vapor, but this happens in a completely continuous way. The standard assumption in thermostatics is that the order parameter is a density or inverse density (e.g., specific volume), and the control parameter is its conjugate (e.g., pressure). But in percolation, the standard choice of order parameter is the fraction $S_{\max}/N$ of sites belonging to the giant cluster, while the control parameter is usually also a density—the density of occupied sites (bonds) in site (bond) percolation. Although this choice is legitimate, it can obscure the notion of first- versus second-order transitions, since other choices more in line with thermostatics can lead to different conclusions. This might explain why previous works on first-order percolation transitions were not recognized as such in the recent literature.

II. THE GENERALIZED EPIDEMIC MODEL: COMPLEX CONTAGION TREATED AS A STOCHASTIC PROCESS

Although the epidemic model of Ref. [30] is formulated as a continuum field theory, the situation becomes more clear on a lattice. Consider a process where the probability of a given site becoming infected (or invaded) by one of its neighbors depends on the number of previous attempts by other neighbors. Once a site is infected, it tries once to infect every one of its not yet infected neighbors. Denote by p_k the probability that an infection succeeds, if the attacked site has already fended off k previous attacks. If every attack increases the strength of the defender, p_k decreases with k, otherwise (if it weakens it), p_k increases. Site percolation is described by $p_0 > 0$ and $p_k = 0$ for $k \geqslant 1$: If the first attack does not succeed, all later attempts are futile. Bond percolation is described by $p_k = p$ for all $k \geqslant 0$. Ordinary (second-order) percolation is observed whenever p_k decreases with k (see also [43]), but the transition switches to first order when p_k increases sufficiently fast. In that case, infected clusters fill in most holes and bays, while protrusions are avoided—thereby making the clusters compact with rough but nonfractal surfaces. (The same effect is caused by high surface tension compared to disorder at the cluster-void interface in random media). Detailed predictions for the tricritical behavior in terms of an $\epsilon = 5 - d$ expansion were given in [30].

A. The GEP on random graphs

Although Dodds *et al.* [36,37] assume a somewhat more complex mechanism of infection, their basic model can be mapped onto a sparse random graph model where each node with n neighbors in the giant cluster is itself in the giant cluster with probability q_n. This is precisely the mean-field (random graph) version of the above model, if $q_1 = p_0$ and $q_{n+1} = q_n + (1 - q_n)p_n$ [44]. Due to the absence of short loops in this case, the condition for tricriticality (transition between classes I and II in [36,37]) simplifies to

$$q_2 = 2q_1, \tag{1}$$

with no restriction on any q_n with $n \geqslant 3$. Since the derivation of this in [36,37] is somewhat involved and obscures the relationship to the GEP as defined in [30], a simple proof of Eq. (1) is given Appendix A.

B. The GEP on regular lattices: tricritical behavior and rough pinned surfaces

In the present work we studied in detail the case where $p_k \equiv p$ is the same for all $k > 0$, while p_0 is different. A technical advantage of this choice is that we have to distinguish only between four types of sites (virgin, attacked but still not infected, infected, and removed), which allows one to store the type in two bits and to simulate larger lattices. Phase diagrams for simple (hyper-) cubic lattices and for random regular graphs are shown in Fig. 1. To the left of the curves, no infinite clusters exist, while such clusters do exist to their right. Since percolation thresholds on lattices scale as $p_c \sim 1/(2d - 1)$

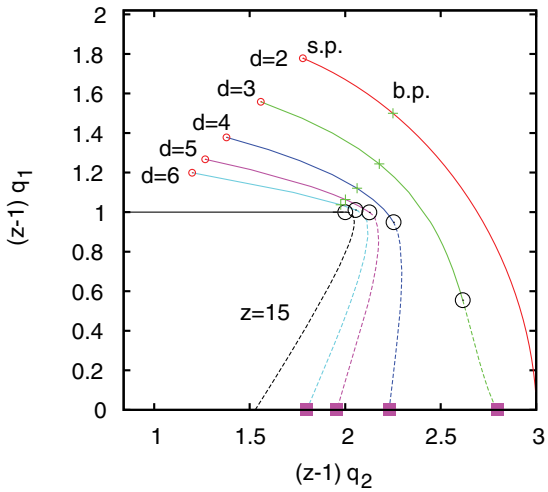

FIG. 1. (Color online) Phase diagrams for the generalized epidemic process where infection of a site succeeds with probability p_0 in the first encounter with an infected neighbor, while it succeeds with chance p in all later encounters. Following [36], we use instead of p_k the probabilities $q_1 = p_0$ and $q_2 = p_0 + (1 - p_0)p$ that an infection has occurred after two encounters. Since percolation thresholds on regular graphs are roughly $\propto 1/(z - 1)$ for large degree z, we use $(z - 1)q_n$ for the two axes. The curves labeled by $d = 2$ to $d = 6$ correspond to d-dimensional hypercubic lattices, where $z = 2d$, while the curve labeled "$z = 15$" is for random (i.e., locally loopless) networks. All curves start at the site percolation point $q_2 = q_1$ (small red circles). The bond percolation points (green crosses) are at $q_2 = (2 - q_1)q_1$. For large d they approach the tricritical points (big black circles) that converge to the point (2,1) for large k. The percolation transitions are first order below the tricritical points, and second order above. For $d = 2$ there is no tricritical point (i.e., clusters and their surfaces are always fractal). In the first-order regime (dashed curves), surfaces develop strong overhangs and seem for $d = 3$ *not* to be described by models where these overhangs are neglected (in particular when $q_1 = 0$ (magenta squares), but they seem to be in the standard universality class of self-affine pinned rough surfaces for $d > 3$.

for large d, we used $(z-1)q_1$ and $(z-1)q_2$ as coordinates in Fig. 1, where z is the coordination number. All curves start at site percolation ($p_1 = 0$, $q_1 = q_2 = p_0$), since we do not consider here antagonistic effects (i.e., two attacks together cannot have less success than a single one). Tricritical points are marked by circles. There is no tricricital transition in $d = 2$ [33] (i.e., isotropic rough 1-d surfaces are always fractal). For large dimensions, the lattice results converge to those for regular random graphs with degree $z = 2d$, as short loops become less and less important with increasing d.

Previously, most studies of pinned rough surfaces were either done for the random field Ising model at zero temperature [32,33,45–47] (which is indeed a special case of GEP [33,48], but not the most convenient one for simulations), or for models where overhangs are neglected. In the latter case the surface can be described by a single-valued self-affine function [49–51]. This makes it much easier to study both numerically and analytically, but the neglect of overhangs is not guaranteed to be justified. The critical exponents obtained in [49–51] seem to agree with simulation results for the random field Ising model [45], but the latter have large uncertainties. Our preliminary results indicate that surface properties in the first-order regimes (i.e., below the tricritical points, but with $q_1 = 0$) are for $d > 3$ indeed in the same universality class of surfaces without overhangs, but not $d = 3$. There the pinned surfaces seem to be rougher than predicted by [49–51], but much more detailed studies are needed and will be reported elsewhere [52].

The case $q_1 = 0$, where at least two infected neighbors are needed for a site to become infected, is similar to bootstrap percolation [53,54]. There, epidemics can neither spread from single sites nor from surfaces with Miller indices $(1,0,0\ldots)$, but they can spread from surfaces with Miller indices $(1,1,1\ldots)$. This means also that no infinite epidemic can spread from an initial distribution of infected sites confined within a finite region. Nevertheless, at least for $d > 3$ there is a critical value of q_2 above which infinite clusters are self-supported, and spreading from an infinite $(1,1,1\ldots)$ surface seems to be in the same universality class of self-affine surfaces as for $q_1 > 0$. Again, the situation is less clear for $d = 3$, where the spreading from a $(1,1,1)$ surface definitely is not in this universality class [52].

For the simple cubic lattice, simulations show that the tricritical point for this model is at $p_0 = 0.111(2)$ and $p_k = 0.464(8)$ for $k > 0$. Results of such simulations for epidemics starting from a single infected site are shown in Fig. 2, where $n(t)$ is the number of sites newly infected at time t. For OP, $n(t)$ increases as a power law t^{η} with $\eta \approx 0.35$ [1], and it decreases at the tricritical point as $n(t) \sim t^{\eta_s}$ with $\eta_s = -0.70(1)$. This is in stark contrast to the prediction $\eta_s \approx 0.05$ of [30]. The tricritical point and OP are the only cases where $n(t)$ shows a power law. For critical percolation with $p_0 > 0.111$ the behavior crosses over to the OP scaling, while for $p_0 < 0.111$ the data are compatible with a stretched exponential at the transition line (see lowest three curves in Fig. 2). Analogous plots for the probability $P(t)$ that the epidemic survives at least t time steps and for its average squared radius $R^2(t)$ are given in Appendix B. They give $\delta_s = 1.49(2)$ and $z_s = 1.205(4)$, where δ_s and z_s are defined via $P(t) \sim t^{-\delta_s}$ and $R^2(t) \sim t^{z_s}$. The predictions of [30] are $\delta_s \approx 0.87$ and $z_s \approx 1.06$. Again, the agreement is far from perfect, although the changes from the OP critical exponents are in the right directions. More details are given in Appendix B and in [52]. For the completely analogous case of directed percolation (SIS epidemics), see [55–57].

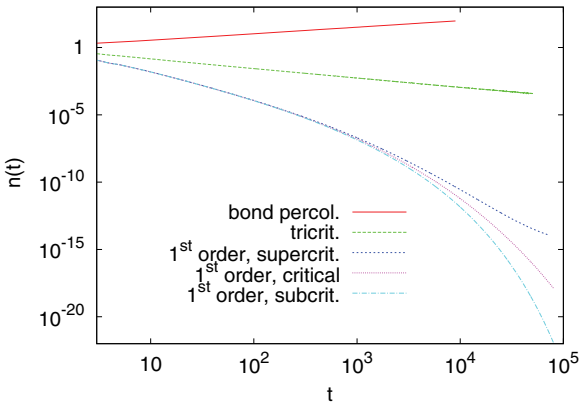

FIG. 2. (Color online) Time dependence of the activity $n(t)$ at five different pairs (p_0,p) where $p_k = p$ for all $k \geqslant 1$, for the generalized epidemic process on the simple 3-d cubic lattice starting from a single infected site. The uppermost (red) curve is for $p_0 = p = 0.2488\ldots$, which is critical bond percolation. The middle (green) curve is for the tricritical point $(p_0,p) = (0.111,0.464)$ [i.e., $(q_1,q_2) = (0.111,0.523)$]. Within the resolution of the figure, both these lines are straight. The lowest three curves are near the first-order (depinning) transition line $(p_0,p) = (0.07,0.792318 + \Delta)$, where $\Delta = 0$ (magenta), $+0.00022$ (dark blue), and -0.00022 (light blue). Statistical error bars are all smaller than the line widths.

III. COOPERATIVE PERCOLATION IN HAMILTONIAN RANDOM GRAPH MODELS

The above discussion suggests that cooperativity in finite temperature equilibrium systems may also lead to discontinuous percolation transitions. Indeed, the mean-field percolation transition corresponds to the emergence of the giant component in ER random graphs, where links appear *independently* with probability p [41]. The ER random graph is the simplest "exponential model" [58–60]. In this approach one considers graphs G with N nodes, where the probability for a given graph is defined by the Boltzmann-Gibbs equilibrium formula,

$$P(G;\theta_1,\theta_2,\ldots) = \frac{1}{Z} e^{-H(G;\theta_1,\theta_2,\ldots)}, \tag{2}$$

with $Z = \sum_G e^{-H(G;\theta_1,\theta_2,\ldots)}$. Here H is the Hamiltonian, $\{\theta_1,\theta_2,\ldots\}$ represents a set of control parameters, and we have set $\beta \equiv 1/kT = 1$. More precisely, we assume that H is a sum of bilinear terms,

$$H(G;\theta_1,\theta_2,\ldots) = \sum_{\alpha} \theta_\alpha A_\alpha(G), \tag{3}$$

where each A_α is an observable ("statistic") of the graph, and θ_α is the associated chemical potential. Typically, each A_α represents the total number of small subgraphs (links, triangles, p stars, four cliques,...,) in the graph.

Models of this type have been popular in mathematical sociology [38,60], although they tend to be unrealistic. In many cases, such models reduce to equivalent ER graphs without

clustering and are trivial, apart from the usual, nontrivial dependence of the observables A_α on the control parameters θ_α [61].

The Hamiltonian for the ER model is

$$H_{\mathrm{ER}}(G;\theta) = \theta L(G), \tag{4}$$

where $L(G)$ is the number of links in G and $\theta = \ln[(1-p)/p]$. It exhibits a percolation transition at $p = 1/N$ (when $N \to \infty$) [41], thus the critical value of θ is

$$\theta_p = \ln N. \tag{5}$$

In the following, we study the two-star model [40] with

$$H_{\text{two-star}}(G;\theta,J) = \theta L(G) - \frac{J}{N} n_2(G). \tag{6}$$

Here $n_2(G)$ is the total number of "two stars" (i.e., pairs of links attached to the same node). We also consider the Strauss model [38,39] with

$$H_{\mathrm{Strauss}}(G;\theta,B) = \theta L(G) - \frac{B}{N} n_\Delta(G), \tag{7}$$

where $n_\Delta(G)$ is the total number of distinct triangles (i.e., of loops of length 3). In terms of the degree sequence $\{k_i, i = 1 \ldots N\}$,

$$L(G) = \frac{1}{2}\sum_{i\in G} k_i, \quad \text{and} \quad n_2(G) = \frac{1}{2}\sum_{i\in G} k_i(k_i-1), \tag{8}$$

while $n_\Delta(G)$ depends also on degree correlations.

For a typical (nonsparse) graph L increases quadratically with N, while both n_2 and $n_\Delta \sim N^3$. This is why J/N and B/N are used as control parameters in Eqs. (6) and (7) instead of J and B. The two-star model has, for any $\theta > 2$, a first-order transition in the density of links at $J^*(\theta)$ and strong hysteresis. The results of [40], together with a standard Maxwell construction, show that

$$J^*(\theta) = \theta. \tag{9}$$

The line of first-order transitions terminates at the critical point $\theta_c^* = J_c^* = 2$. [We neglect here all terms that are $\mathcal{O}(1/N)$ relative to the leading ones]. Similarly, for the Strauss model a first-order transition in the link density $p = \langle L\rangle/N$ occurs for any $\theta \gtrsim 0.81$ [39]. This time it is more complicated to obtain the exact transition line $B^*(\theta)$, but one can show that (see Appendix C)

$$B^*(\theta) \approx 3\theta \quad \text{for } \theta \gg 1, \tag{10}$$

with a critical point at $p_c^* = 2/3, B_c^* = 27/8 = 3.375$, and $\theta_c^* = 3/2 - \ln(2) \approx 0.807$.

For both models, a giant component exists in both the high and low link density phases, whenever $\theta = \mathcal{O}(1)$. Thus the density transition happens when they are already percolating, as long as θ is finite. In order to reach a percolation transition one has to take $\theta \sim \ln N$ to get a sparse graph. In this regime the above estimates for the density transitions are still valid. Moreover, when $B < B^*$ or $J < J^*$, respectively, the second terms in the Hamiltonians [Eqs. (6) and (7)] have no influence on the percolation transition, for $N \to \infty$. This is illustrated for the two-star model in Fig. 3, where we show numerical results averaged over 50 hysteresis loops for a network with $N = 2000$ and $J = 3.0$. The density transition (monitored via the average degree) indeed appears to be first order with strong hysteresis, while the percolation transition (monitored via $\langle S_{\max}\rangle/N$) shows no hysteresis and is *exactly* the same as for ordinary ER networks.

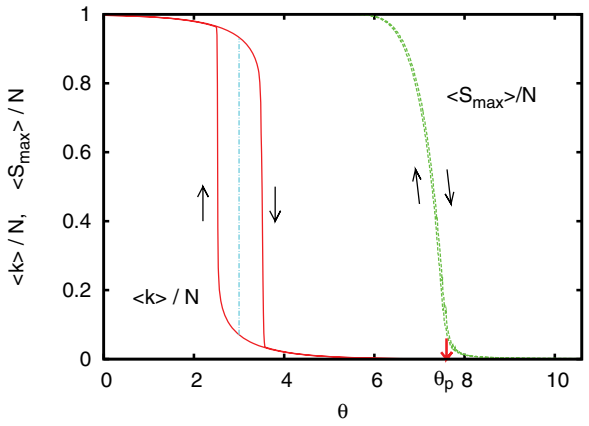

FIG. 3. (Color online) Hysteresis loops for the two-star model for fixing the two-star control parameter at $J = 3$ and sweeping the control parameter θ for links. The loop on the left (red) is for the normalized average degree, while the one on the right (green) is for the percolation order parameter $\langle S_{\max}\rangle/N$. The vertical dashed (blue) line is the Maxwell prediction for the true density transition. The curve for $\langle S_{\max}\rangle/N$ shows practically no hysteresis and agrees within error with the one for OP. The percolation threshold $\theta_p = \ln N$ is indicated on the x axis. The rounding of the green curve near θ_p is a finite size effect ($N = 2000$).

When $J > \ln N$ (or $B > \ln N$, respectively) this scenario breaks down because the true equilibrium state at the ER percolation threshold, θ_p, is a dense graph that consists of a single giant component. Although the equilibrium network percolates at θ_p, a hysteresis loop starting at $\theta > J$ begins with a sparse nonpercolating graph, and due to metastability the effect of J (or B) is not seen until one passes the ER percolation threshold—provided that it remains in the metastable region. This scenario is illustrated in Fig. 4 for $J = \theta_p = \ln N$. Now the hysteresis loop for $\langle k\rangle/N$ is quite wide. The hysteresis loop

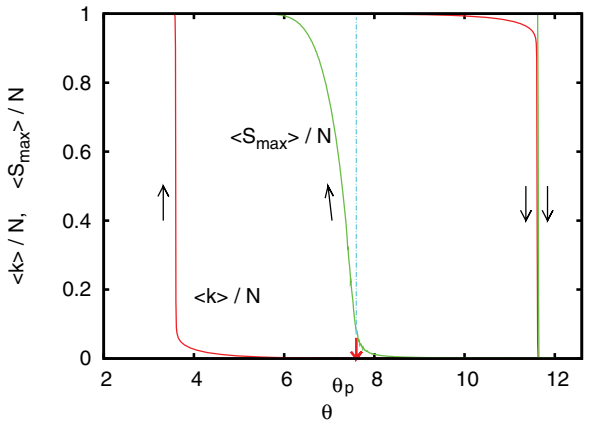

FIG. 4. (Color online) Analogous to Fig. 3, but for $J = \theta_p = \ln N = 7.601$. This time the percolation threshold coincides with the true (Maxwell) density transition. As a consequence, also the curve for $\langle S_{\max}\rangle/N$ shows hysteresis, with a continuous lower branch and a discontinuous upper branch ($N = 2000$).

for $\langle S_{\max}\rangle/N$ shows the ordinary ER percolation shape on its lower branch, while it follows the discontinuous behavior of $\langle k\rangle/N$ on the upper (return) branch. To our knowledge, such a mixed-order hysteresis loop has not been observed before, although a similar phenomenon was seen in heterogeneous k-core percolation [42]. But since the latter is not Hamiltonian and does not allow for the notion of thermal equilibrium, the two cannot be strictly compared.

IV. CONCLUSIONS

As we already mentioned and as was pointed out repeatedly before [39,40,61], the two-star and Strauss models are not realistic for real world applications. Accordingly, our demonstration that they exhibit both second- and first-order percolation transitions should be considered only as a proof that this phenomenon exists in equilibrium. More interesting examples can be easily suggested. A class of models that come into mind are random graphs (i.e., mean-field type) where not only the number of nodes but also the number of links is set by hard constraints ("microcanonical models") [62]. A model with two control parameters (B and J) studied in [63] exhibits the zoo of metastable states, but it seems that most of these states are still too extreme to be physical. A further step in this direction could be to fix not only the average degree, but to fix the entire degree distribution, either by soft [64] or by hard [65] constraints.

A more realistic class of Hamiltonian models with first-order phase transitions could be spatially embedded (e.g., finite dimensional lattice) systems. Such models have not been studied much in the social science literature, although it is well known that, for instance, spatial structure is essential to maintain diversity in ecosystems. We believe that such models might provide a suitable mixture of structure and randomness to reveal important features of real, complex networks, including presumably percolation transitions of both continuous and discontinuous type.

In summary, we have shown that various percolation models can be naturally generalized such that they switch from ordinary, continuous behavior at the transition point to discontinuous ("first-order") behavior, as some parameter is varied. This parameter usually is a measure of cooperativity in linking or "infecting" sites (the probability for sites to get linked is increased by other links already present), such that the percolation transition is more abrupt when cooperativity is high. We present a unified treatment including examples that range from social dynamics to condensed matter physics, and we also show that analogous phenomena occur both in stochastic dynamics out of equilibrium as well as in a Gibbs-Boltzmann equilibrium framework. We also simplify the dynamical description of the social contagion process introduced by Dodds and Watts [36], clarifying thereby its relation to percolation and to the generalized epidemic process defined in [30].

In condensed matter physics, the first-order percolation transition is just the depinning transition of driven interfaces in disordered media at zero temperature. Treating it also in our unified framework not only allows us to study in detail the tricritical point (where we found for $d = 3$ striking disagreement with theoretical predictions), but also to numerically investigate more efficiently a model for pinned surfaces in which overhangs are fully included and hence the rotational symmetry of the growth process is not explicitly broken at scales much less than the system size. In this latter context, the most important (but so far only preliminary) result we find is that overhangs are indeed crucial for such surfaces, and that all existing theories for critically pinned rough surfaces (which neglect overhangs and are based on a single-valued "height function") might be obsolete, not being relevant to the most interesting physical case of isotropic media.

APPENDIX A: THE EPIDEMIC THRESHOLD IN THE DODDS-WATTS SOCIAL CONTAGION MODEL

Since the original derivation of the result $q_2 = 2q_1$ by Dodds and Watts [36] is somewhat cumbersome and involves more than a minimal set of assumptions, we give here a simpler derivation following the typical arguments for epidemic thresholds via consistency conditions [27,66,67]. We start by recalling the condition for the threshold of the standard epidemic process that leads to ordinary percolation, and we then modify a suitable reformulation so that it also applies to the more general case with different infection probabilities p_k. We finally obtain the critical line and the tricritical point by straightforward algebra.

Let us call S the probability that a node at one end of a randomly chosen link gets infected during an epidemic process on a sparse random network with degree distribution P_k. If the infection can pass through any link with probability p, then the locally treelike structure of the network results in the consistency condition [66,67],

$$1 - S = z^{-1} \sum_{k=1}^{\infty} k P_k (1 - pS)^{k-1}, \tag{A1}$$

where $z = \langle k\rangle = \sum_k k P_k$. We write this as

$$F_{\rm OP}(S) \equiv \sum_{k=1}^{\infty} k P_k (1 - pS)^{k-1} + z(S - 1) = 0 \tag{A2}$$

(the subscripts stand for "ordinary percolation"). The percolation threshold is then defined by

$$F_{\rm OP}(0) = F'_{\rm OP}(0) = 0, \tag{A3}$$

where $F'_{\rm OP}(S) \equiv dF_{\rm OP}/dS$. Straightforward calculations give [41,66,67]

$$p_c = \frac{\langle k\rangle}{\langle k(k-1)\rangle}. \tag{A4}$$

We also notice that $F''_{\rm OP}(0) > 0$.

In order to modify this to arbitrary infection probabilities p_n for attacks following n previous attacks, we first rewrite Eq. (A2) such that contributions from different numbers of infected neighbors are separated. In order to do this we write $1 - pS = (1 - S) + (1 - p)S$, such that the first term is the probability that the considered node is not infected, while the second terms is the probability that it is infected, but it cannot infect its neighbor since the link cannot be passed. Similarly

we write

$$(1-pS)^k = \sum_{n=0}^{k-1} \binom{k-1}{n} [(1-p)S]^n (1-S)^{k-n-1}, \quad \text{(A5)}$$

such that each term in the sum corresponds to exactly n infected neighbors. The modification to the generalized process is now obvious: We just have to replace the power $(1-p)^n$ by $(1-p_0)(1-p_1)\dots(1-p_{n-1})$. Alternatively, we can replace it by $1-q_n$ where q_n is the probability that n attacks succeed in infecting the site. The formulations using p_n and q_n are fully equivalent.

Making this modification in Eq. (A2) results in

$$F_{\rm GEP}(S) = \sum_{k=1}^{\infty} k P_k \sum_{n=0}^{k-1} \binom{k-1}{n} \times [1-q_n] S^n (1-S)^{k-n-1} + z(S-1), \quad \text{(A6)}$$

where GEP stands for "generalized epidemic process." As before, the condition for criticality is

$$F_{\rm GEP}(0) = F'_{\rm GEP}(0) = 0, \quad F''_{\rm GEP}(0) > 0, \quad \text{(A7)}$$

while the tricritical point is given by

$$F_{\rm GEP}(0) = F'_{\rm GEP}(0) = F''_{\rm GEP}(0) = 0, \quad \text{(A8)}$$

Evaluating the derivatives is straightforward and gives [36]

$$q_2 = 2q_1, \quad \text{(A9)}$$

and q_1 is given by Eq. (A4). Notice that the location of the tricritical point does not depend on any q_n with $n > 2$, and its existence does not put any constraints on them.

In the first-order regime, the threshold condition for an epidemic is

$$F_{\rm GEP}(S) = F'_{\rm GEP}(S) = 0, \quad \text{(A10)}$$

which depends nontrivially both on the degree distribution and on all p_n (or all q_n). For regular graphs with degree z (i.e., $P_k = \delta_{k,z}$) and $p_n = p$ for all $n \geqslant 1$ it approaches in the limit $z \to \infty$ the linear relation $q_2 = 1/z + p_1$. For $z = 15$, numerical solution of Eq. (11) gives the line plotted in Fig. 1.

APPENDIX B: DETAILS ON THE SIMULATION OF TRICRITICAL AND FIRST-ORDER PERCOLATION ON 3-*d* LATTICES

All simulations were done on simple cubic lattices, with synchronous (discrete time) updates. We followed the spreading of epidemics that started either with point seeds or with the seed consisting of an entire infected plane. In the former we used lattices of size up to 2048^3 and checked that clusters never reached the boundary. For small values of p_0, when growth from a point seed has a very high chance to die out, we used PERM [68] to grow clusters even if their probability was as low as 10^{-300}. For simulations initiated from an entire infected plane (results of which are not shown here but are used, in addition, to better estimate (tri-)critical points) we used lattices of sizes up to $4096^2 \times 2048$ with helical lateral boundary conditions. In that case we also implemented multispin coding in order to use only 2 bits to store the status of any site. We also recycled memory in order to grow epidemics that spread

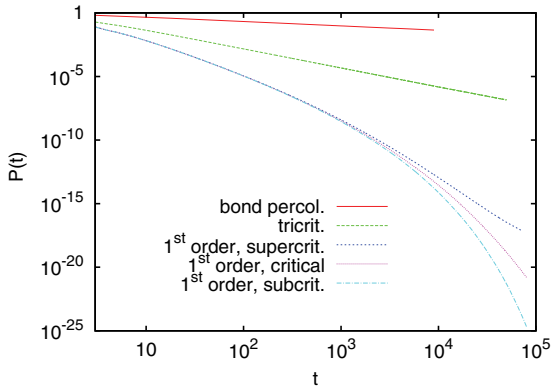

FIG. 5. (Color online) Log-log plot analogous to Fig. 1, but for $P(t)$ instead of $n(t)$. Here $P(t)$ is the probability that an epidemic started with a single infected site is still growing after t time steps. The decay follows a power law both at OP and at the tricritical point [with exponent $-1.49(2)$ for the latter], while it seems to follow a stretched exponential at the first-order (i.e., rough surface depinning) transition point. Again the central one of the three lowest curves (for $p_0 = 0.07$) corresponds to depinning.

far from the initial infected boundary, by overwriting older parts of the cluster that were no longer growing. This enlarges the effective lattice size to $4096^2 \times L_z$ with $L_z \gg 2048$. The precise thickness that we must not overwrite depended of course on the actual roughness of the growing surface. It was always checked that the cluster could grow without improperly interfering with some of its older parts.

Further details will be given elsewhere [52]. They will concern statistics, the precise methods used to estimate exact tricritical properties, critical exponents for rough pinned surfaces, and the behavior in dimensions different from 3. Here we present just two more figures (Figs. 5 and 6), similar to

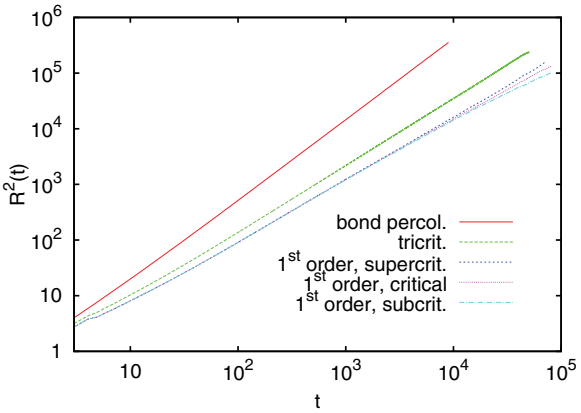

FIG. 6. (Color online) Analogous to Figs. 1 and 5, but for $R^2(t)$ which is the average distance of active (i.e., newly infected) sites from the seed. In the first-order regime the cluster grows very slowly, and $R^2(t)$ should be dominated by the motion of their center of mass. Since clusters can grow only into new (not previously infected) areas, this motion should be essentially a self-avoiding random walk. Our estimate for the critical exponent is consistent with this, although there are large finite time corrections that make $R^2(t)$ grow even less fast than t for very long times, in particular for p below the transition. At the tricritical point, $R^2(t)$ is a power law with exponent 1.205(4).

Fig. 1, that show the survival probability $P(t)$ and the average squared radius $R^2(t)$ of newly infected sites, measured from the starting point of the epidemic. They show power-law behavior at the tricritical point (straight lines on log-log plots), with exponent values given in the main text.

A detailed comparison of our results with the field theoretic predictions of [30] will also be given in [52]. Here we just mention that our results for the critical exponents are qualitatively similar (the changes relative to the exponents for OP go in the right directions), but the agreement is far from perfect. The biggest disagreement is for η_s, defined via $n(t) \sim t^{\eta_s}$. While a positive value,

$$\eta_s = \left(\frac{1}{3} + \frac{4-\sqrt{3}}{\pi}\right)\frac{\epsilon}{45} + O(\epsilon^2), \tag{B1}$$

with $\epsilon = 5 - d = 2$, was predicted in [30], we found $\eta_s = -0.702(10)$.

APPENDIX C: THE STRAUSS MODEL

We start from Eqs. (5) and (6) of Ref. [39], which read in our notation,

$$p = \frac{1}{e^{\theta - Bq(1-2/N)} + 1}, \tag{C1}$$

and

$$q = \frac{1 + (e^{B/N} - 1)p}{(e^{\theta - Bq(1-3/N)} + 1)^2 + (e^{B/N} - 1)p}. \tag{C2}$$

Here p is the link density and q is defined in [39]. In the limit $N \to \infty$ and $B, \theta \ll N$ of interest to us, these simplify to

$$p = \frac{1}{e^{\theta - Bq} + 1}, \tag{C3}$$

and

$$q = \frac{1}{(e^{\theta - Bq} + 1)^2} = p^2. \tag{C4}$$

Combining these gives an equation for p in terms of B and θ which we can write as

$$F(p) \equiv e^{\theta - Bp^2} + 1 - \frac{1}{p} = 0. \tag{C5}$$

This equation can have four outcomes (see Fig. 7):

(a) one simple solution, corresponding to one single phase [i.e., no phase coexistence; Fig. 7(a)];

(b) three different solutions (two stable + one unstable), corresponding to phase coexistence [Fig. 7(b)];

(c) one single plus one doubly degenerate solution, corresponding to the boundaries of the coexistence region [Figs. 7(c1) and 7(c2)]; and

(d) one triply degenerate solution, corresponding to the critical point [Fig. 7(d)].

The critical point is thus obtained from $F(p) = F'(p) = F''(p) = 0$, leading to the values quoted in the main text.

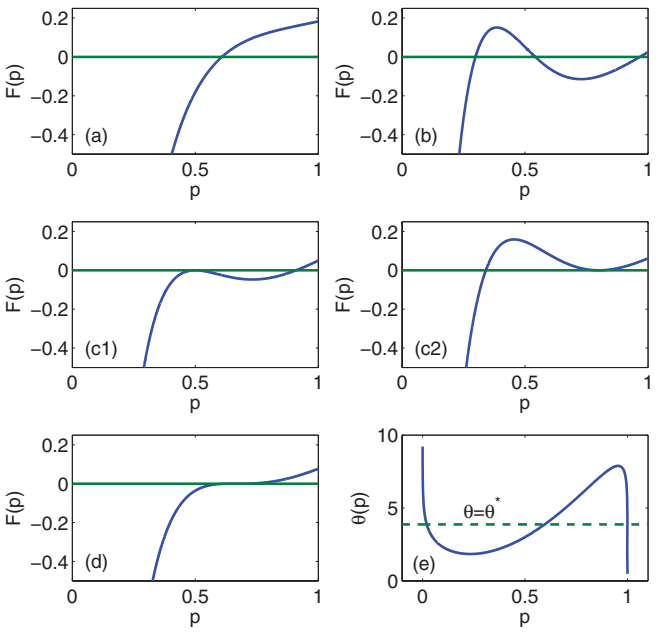

FIG. 7. (Color online) Panels (a)–(d) illustrate the cases (a)–(d) for the possible solutions of $F(p) = 0$. Panel (e) illustrates the Maxwell construction. The function $\theta(p)$ is given by Eq. (C8), and the dashed horizontal line is placed such that the two areas between it and the curve $\theta = \theta(p)$ are equal.

The boundaries of the bistable region are given parametrically by

$$B = \frac{1}{2(1-p)p^2}, \quad \theta = \ln(1/p - 1) + \frac{1}{2(1-p)}, \tag{C6}$$

which give asymptotically for large θ,

$$B_-(\theta) \approx \theta\ , \quad B_+ \approx \exp(2\theta), \tag{C7}$$

for the lower (upper) boundaries in a plot of B versus θ (see Fig. 2 of [39]).

The actual transition curve $B^*(\theta)$, or rather $\theta^*(B)$, is obtained from a Maxwell construction: For some given value of $B > B_c^*$, we first obtain θ as a function of p from Eq. (C5),

$$\theta(p) = Bp^2 + \ln(1/p - 1). \tag{C8}$$

For any θ_0 in the coexistence region, the equation $\theta(p) = \theta_0$ has three roots $p_1 < p_2 < p_3$. The transition point $\theta^*(B)$ is then given by

$$\int_{p_1}^{p_3} dp\ [\theta(p) - \theta^*(B)] = 0. \tag{C9}$$

For large B, the curve of $\theta(p)$ versus p tends (except near the points $p = 0$ and $p = 1$) to a parabola, which gives in this limit $\theta^*(B) \approx B/3$ as stated in the main text.

[1] D. Stauffer and A. Aharony, *Introduction to Percolation Theory* (Taylor & Francis, London, 1994).

[2] D. Achlioptas, R. M. D'Souza, and J. Spencer, Science **323**, 1453 (2009).

[3] R. A. da Costa, S. N. Dorogovtsev, A. V. Goltsev, and J. F. F. Mendes, Phys. Rev. Lett. **105**, 255701 (2010).

[4] O. Riordan and L. Warnke, Science **333**, 322 (2011).

[5] P. Grassberger, C. Christensen, G. Bizhani, S.-W. Son, and M. Paczuski, Phys. Rev. Lett. **106**, 225701 (2011).

[6] H. K. Lee, B. J. Kim, and H. Park, arXiv:1103.4439 (2011).

[7] A. Vespignani, Nature (London) **464**, 15 (2010).

[8] E. J. Friedman and A. S. Landsberg, Phys. Rev. Lett. **103**, 255701 (2009).

[9] R. M. Ziff, Phys. Rev. Lett. **103**, 045701 (2009).

[10] R. M. Ziff, Phys. Rev. E **82**, 051105 (2010).

[11] F. Radicchi and S. Fortunato, Phys. Rev. Lett. **103**, 168701 (2009).

[12] F. Radicchi and S. Fortunato, Phys. Rev. E **81**, 036110 (2010).

[13] R. M. D'Souza and M. Mitzenmacher, Phys. Rev. Lett. **104**, 195702 (2010).

[14] H. D. Rozenfeld, L. K. Gallos, and H. A. Makse, Eur. Phys. J. B **75**, 305 (2010).

[15] S. S. Manna and A. Chatterjee, Physica A **390**, 177 (2009).

[16] A. A. Moreira, E. A. Oliveira, S. D. S. Reis, H. J. Herrmann, and J. S. Andrade Jr., Phys. Rev. E **81**, 040101 (2010).

[17] N. A. M. Araújo and H. J. Herrmann, Phys. Rev. Lett. **105**, 035701 (2010).

[18] W. Chen and R. M. D'Souza, Phys. Rev. Lett. **106**, 115701 (2011).

[19] Y. S. Cho, B. Kahng, and D. Kim, Phys. Rev. E **81**, 030103 (2010).

[20] Y. S. Cho, J. S. Kim, J. Park, B. Kahng, and D. Kim, Phys. Rev. Lett. **103**, 135702 (2009).

[21] Y. S. Cho, S.-W. Kim, J. D. Noh, B. Kahng, and D. Kim, Phys. Rev. E **82**, 042102 (2010).

[22] L. Tian and D.-N. Shi, Phys. Lett. A **376**, 286 (2012).

[23] J. Nagler, A. Levina, and M. Timme, Nature **7**, 265 (2011).

[24] H. Hooyberghs and B. Van Schaeybroeck, Phys. Rev. E **83**, 032101 (2011).

[25] S. V. Buldyrev, R. Parshani, G. Paul, H. E. Stanley, and S. Havlin, Nature (London) **464**, 1025 (2010).

[26] R. Parshani, S. V. Buldyrev, and S. Havlin, Phys. Rev. Lett. **105**, 048701 (2010).

[27] S.-W. Son, G. Bizhani, C. Christensen, P. Grassberger, and M. Paczuski, Europhys. Lett. **97**, 16006 (2012).

[28] S. Boettcher, V. Singh, and R. M. Ziff, Nat. Comm. **3**, 787 (2012).

[29] T. Ohtsuki and T. Keyes, Phys. Rev. A **36**, 4434 (1987).

[30] H.-K. Janssen, M. Müller, and O. Stenull, Phys. Rev. E **70**, 026114 (2004).

[31] Janssen *et al*. called this the generalized general epidemic process (GGEP), in order to distinguish it from the general epidemic process [D. Mollison, J. Royal Statist. Soc. B **39**, 283 (1977)]. The latter is now usually called a susceptible-infected-removed (SIR) epidemic, while a "simple epidemic" in the notation of Mollison is now called SIS. We feel thus free to use the simpler acronym GEP for the generalized process.

[32] M. Cieplak and M. O. Robbins, Phys. Rev. Lett. **60**, 2042 (1988); N. Martys, M. Cieplak, and M. O. Robbins, *ibid*. **66**, 1058 (1991); N. Martys, M. O. Robbins, and M. Cieplak, Phys. Rev. B **44**, 12294 (1991); H. Ji and M. O. Robbins, *ibid*. **46**, 14519 (1992); C. S. Nolle, B. Koiller, N. Martys, and M. O. Robbins, Phys. Rev. Lett. **71**, 2074 (1993).

[33] B. Drossel and K. Dahmen, Euro. Phys. J. B **3**, 485 (1998).

[34] Note that the co-appearance of first-order bulk transitions with continuous surface transitions was discussed already in [69].

[35] D. J. Watts, PNAS **99**, 5766 (2002).

[36] P. S. Dodds and D. J. Watts, Phys. Rev. Lett. **92**, 218701 (2004).

[37] P. S. Dodds and D. J. Watts, J. Theor. Biol. **232**, 587 (2005).

[38] D. Strauss, SIAM Rev. **28**, 513 (1986).

[39] J. Park and M. E. J. Newman, Phys. Rev. E **70**, 026136 (2005).

[40] J. Park and M. E. J. Newman, Phys. Rev. E **70**, 066146 (2004).

[41] B. Bollobás, *Random Graphs* (Cambridge University Press, Cambridge, 1985).

[42] G. J. Baxter, S. N. Dorogovtsev, A. V. Goltsev, and J. F. F. Mendes, Phys. Rev. E **83**, 051134 (2011).

[43] F. J. Pérez-Reche, J. J. Ludlam, S. N. Taraskin, and C. A. Gilligan, Phys. Rev. Lett. **106**, 218701 (2011).

[44] Strictly spoken this is only true for static (i.e., percolation in the narrow sense) aspects at threshold. Dynamics and the behavior above the threshold are different in both models, since the memory about previous contacts with infected neighbors is short lived in [36,37], while it is long lived (previous attacks are never forgotten) in the model of [30] and in the simulations reported in the next subsection.

[45] L. Roters, A. Hucht, S. Lübeck, U. Nowak, and K. D. Usadel, Phys. Rev. E **60**, 5202 (1999).

[46] B. Koiller and M. O. Robbins, Phys. Rev. B **62**, 5771 (2000).

[47] B. Koiller and M. O. Robbins, Phys. Rev. B **82**, 064202 (2010).

[48] If the distribution of local fields in the random field Ising model is called $P(h)$, the spin-spin coupling is J, and z is the coordination number, then $q_n = \int_{-\infty}^{(2n-z)J} P(h)dh$.

[49] H. Leschhorn, T. Nattermann, S. Stepanow, and L.-H. Tang, Ann. Physik (Leipzig) **6**, 1 (1997).

[50] P. Le Doussal, K. J. Wiese, and P. Chauve, Phys. Rev. B **66**, 174201 (2002).

[51] A. Rosso, A. K. Hartmann, and W. Krauth, Phys. Rev. E **67**, 021602 (2003).

[52] P. Grassberger *et al*. (unpublished).

[53] J. Adler, Physica A **171**, 453 (1991).

[54] Bootstrap percolation on a lattice with coordination number z and with m wetted neighbors needed for support can be mapped onto a GEP with $p_k = \delta_{k,z-m}$, as seen by interchanging wetted and nonwetted sites. Notice that the same interchange was also made in [42], which is the reason why bootstrap percolation is called there an activation and not a pruning process. For completeness we point out that also heterogeneous bootstrap percolation [42] can be mapped onto GEP. The case illustrated in Fig. 1 of [42], for example, corresponds to $p_k = (1-f)\delta_{k,0} + f\delta_{k,2}$.

[55] H.-K. Janssen, J. Phys.: Condens. Matter **17**, S1973 (2005).

[56] S. Lübeck, J. Stat. Phys. **123**, 193 (2006).

[57] P. Grassberger, J. Stat. Mech. (2006) P01004.

[58] P. W. Holland and S. Leinhard, JASA **76**, 373 (1981).

[59] J. Park and M. E. J. Newman, Phys. Rev. E **70**, 066117 (2004).
[60] G. Robins, P. Pattison, Y. Kalish, and D. Lusher, Social Networks **29**, 173 (2007).
[61] S. Chatterjee and P. Diaconis, arXiv:1102.2650 (2011).
[62] J. Berg and M. Lässig, Phys. Rev. Lett. **89**, 228701 (2002).
[63] G. Bizhani *et al*. (unpublished).
[64] J. Park and S.-H. Yook, J. Stat. Mech. (2011) P08008.
[65] D. Foster, J. Foster, M. Paczuski, and P. Grassberger, Phys. Rev. E **81**, 046115 (2010).
[66] M. E. J. Newman, S. H. Strogatz, and D. J. Watts, Phys. Rev. E **64**, 026118 (2001).
[67] M. E. J. Newman, Phys. Rev. Lett. **95**, 108701 (2005).
[68] P. Grassberger, Comp. Phys. Commun. **147**, 64 (2002).
[69] R. Lipowsky, Phys. Rev. Lett. **49**, 1575 (1982).